Materials Research Proceedings 44 (2024) 358-367 https://doi.org/10.21741/9781644903254-38

Hole expansion performance of a medium manganese advanced high-strength steel after hot rolling and intercritical annealing

PLOSILA Pekka[1,a*], KANTANEN Pekka[1,b], HANNULA Jaakko[1,c], JAVAHERI Vahid[1,d], KÖMI Jukka[1,e] and KAIJALAINEN Antti[1,f]

[1]Centre for Advanced Steels Research, Materials and Mechanical Engineering, University of Oulu, Pentti Kaiteran katu 1, 90570 Oulu, Finland

[a]pekka.plosila@oulu.fi, [b]pekka.kantanen@oulu.fi, [c]jaakko.hannula@oulu.fi, [d]vahid.javaheri@oulu.fi, [e]jukka.komi@oulu.fi, [f]antti.kaijalainen@oulu.fi

Keywords: Medium Manganese Steel, Annealing, Retained Austenite, Formability, Stretch-Flangeability

Abstract. This paper investigates the hole expansion behavior of a medium manganese advanced high-strength steel. The study began with vacuum-cast 0.3C–1Si–6Mn–2Al steel, which was subsequently laboratory hot-rolled to a thickness of 4 mm. Intercritical annealing treatments (IAT) were then carried out at temperatures of 650 °C and 700 °C to produce varying fractions of tempered martensite/ferrite and retained austenite (RA). Tensile tests were performed in the longitudinal direction, while hole expansion tests following ISO 16630 were conducted to assess the stretch-flangeability of the IAT materials. Test holes were prepared using punching and wire electrical discharge machining (W-EDM) to examine the effects of different edge conditions. Tensile strength of 1027 MPa and 911 MPa corresponding to a microstructure consisting of RA fraction of 7.5% and 43.3% were obtained at IA temperatures of 650 °C and 700 °C, respectively. Mean hole expansion ratios (HER) with punched holes were relatively low for the given strength levels (3% and 17% for IAT 650 °C and IAT 700 °C, respectively). W-EDM edge condition considerably improved HER but not as much as expected, potentially due to the high inhomogeneity of the microstructure. Further research on optimization of processing and microstructure is required to enhance the poor hole expansion performance of intercritically annealed medium manganese steels.

Introduction

In the automotive sector, utilizing advanced high-strength steels, which offer an enhanced combination of strength and ductility, can result in improvements in cost-effectiveness, weight reduction, and fuel efficiency. This is particularly evident in chassis components. Production of sheet metal components often involves blanking followed by different cold-forming processes. During these forming operations, the blank edges are subjected to various stress and strain conditions. Consequently, there is a potential risk of failure at the cut edge during subsequent stages of production due to the damage and strain hardening present in the sheared edge [1]. The formability of sheared edge becomes an increasingly critical concern as material tensile strength rises.

The ISO 16630 hole expansion test [2] is the most commonly used method for assessing the suitability of sheet metals for forming processes involving stretching of cut edges. In this test, a conical expansion tool is forced into a punched hole until a through-thickness crack occurs. Diameter of the expanded hole after failure is then compared to the initial hole diameter. The test results typically exhibit significant variability and can be greatly influenced by testing conditions, such as cutting clearance, tool shape and wear [3]. Alternative hole preparation methods, such as wire electrical discharge machining (W-EDM) [4,5], demonstrate significant improvement in the

hole expansion performance of high-strength steels. This enhancement is attributed to the prevention of the formation of a highly deformed zone near the edge of the material.

Advanced high-strength steels (AHSS) consist of diverse microstructures, including different fractions of martensite, bainite, ferrite, and retained austenite (RA), which result in varying local ductility. In AHSSs with complex microstructures containing considerable amount of retained austenite, increase in the fraction of RA [6] and fresh martensite [7] have been reported to decrease hole expansion performance.

Medium (4–10%) manganese steel is one of the possible candidates to achieve the requirements of third generation AHSS grades [8]. Beyond desired properties of AHSSs, considerations of industrial manufacturability are crucial in developing new steel grades. In the case of medium manganese steels, the IAT process leverages a substantial fraction of metastable austenite to enhance ductility. The amount of RA is primarily controlled by the intercritical annealing time and temperature at which austenite and ferrite coexist allowing for alloying element partitioning to occur. During IAT carbon (C) and substitutional elements like manganese (Mn) partition from martensite/ferrite to austenite. Both C and Mn are strong austenite stabilizers and an increase in their concentration can result in increasing austenite stability at room temperature [9,10].

Hence, this study aims to evaluate hole expansion performance of a medium manganese advanced high-strength hot-rolled steel after intercritical annealing treatments producing different fractions of tempered martensite/ferrite and particularly different amount of retained austenite. Additionally, effects of shear cutting on the stretch-flangeability of the IAT materials are investigated by comparing punched and wire electrical discharge machined hole edges.

Experimental

Research Materials and Processing. Experimental medium manganese steel containing 0.3C–1Si–6Mn–2Al was designed and vacuum cast into a 65 kg ingot. After the vacuum casting, pieces of around 40 × 80 × 90 mm were cut from the ingot and soaked in a furnace at 1200°C for 2 hours. Subsequently, the steel pieces were laboratory hot-rolled to a thickness of 4 mm with a final rolling temperature (FRT) of 920°C followed by air cooling to room temperature (RT).

After the hot rolling, the steels were annealed in a furnace at intercritical region with temperatures of 650°C and 700°C to produce two test materials with different microstructures; especially with low and high fraction of retained austenite. Holding times at IA temperatures were 10 min, and after IAT the materials were air-cooled to RT.

Base Material Microstructural Investigation. Microstructures of the materials were investigated utilizing a Zeiss Sigma field emission scanning electron microscope (FESEM). The samples were prepared from the rolling direction – normal direction (RD-ND) cross-sections and polished with the standard metallographic sample preparation. Samples were etched with 2% Nital before investigation.

Detailed microstructural features were characterized by employing electron backscatter scanning diffraction (EBSD) detector. EBSD investigations were made with JEOL JSM-7900F FESEM equipped with an Oxford EBSD detector. All samples for EBSD and x-ray diffraction (XRD) were polished to mirror finish using a silica suspension (0.04 μm) in the final step. EBSD samples (RD-ND cross-section) were investigated at quarter thickness of the materials with acceleration voltage of 20 kV and a step size of 0.02 μm. The captured data was post-processed using Oxford AZtecCrystal software.

Retained austenite (RA) fractions were quantified utilizing XRD analysis using a 9 kW Rigaku SmartLab XRD unit operated on a Co-Kα source. XRD analysis was facilitated by PDXL2 analysis software. A de-texturing method was adopted in the XRD measurements, and a Rietveld refinement technique was utilized in the determination of the phase fractions. Volume fractions of RA (XRD) were measured at the material quarter thickness on rolling direction – transverse direction (RD-TD) cross-sections.

Material bulk Vickers hardness was also measured from the FESEM samples using a Zwick ZHU 2.5 universal hardness testing machine. The testing was conducted at material quarter thickness with five measurement points and 98.07 N testing force.

Tensile Testing. Uniaxial tensile tests were performed at room temperature with a Zwick Z100 materials testing machine in accordance with EN ISO 6892-1 [11] utilizing sheet thickness flat specimens with gauge length of 50 mm, parallel length of 75 mm, and width of 12.5 mm. Tensile testing was conducted in the longitudinal direction with 3 repeat specimens. Strain hardening exponents ($n_{4–6}$) were determined from the tensile test data in a plastic strain range between 4% and 6%.

To evaluate local ductility of the investigated materials, thickness strains at fracture of the tensile specimens were investigated. Measurements were conducted on the fracture surfaces of the tensile specimens with a digital microscope (Dino-Lite Edge). The microscope was focused on the thinnest point of the fracture surface. The true plastic thickness strain ($\varepsilon_{p\_a_{min}}$) was calculated with Eq. 1 [12]

$$\varepsilon_{p\_a_{min}} = \ln(a_0/a_{min}), \quad (1)$$

where a_0 is the initial specimen thickness and a_{min} is the specimen thickness at minimum thickness point of the fracture surface.

Hole Expansion Testing. To evaluate stretch-flangeability of the materials, hole expansion tests according to ISO 16630 [2] were performed. 10 mm diameter test holes for the hole expansion testing were prepared using two different methods: punching according to the standard and wire electrical discharge machining (W-EDM) to obtain edges with shear-affected and essentially pre-damage free conditions, respectively. Prior to hole preparation, rolling surfaces of all hole expansion test pieces were sandblasted to remove excess furnace and rolling scale. Punching was conducted according to the ISO 16630 with a 12.5% cutting clearance. Four punched and two W-EDM holes were produced for each material. One unexpanded hole for both punched and W-EDM conditions was reserved for hole edge quality investigations.

Hole expansion tests were conducted at Lapland University of Applied Science in Kemi with an Erichsen universal sheet metal testing machine. For each material, three punched and one W-EDM hole was tested. A conical expansion tool with a 60° tip angle was forced into the hole of the specimen at rate of 15 mm/min. The burr side of the specimen was set facing away of the expansion tool and no lubrication was used. The movement of the expansion tool was stopped as a through-thickness crack was observed in the hole edge by the operator. Hole diameters were determined after the tests with caliper measurements and the limiting hole expansion ratio (HER) was calculated with Eq. 2 [2]

$$HER = \frac{D_h - D_0}{D_0} \times 100, \quad (2)$$

where D_h is the hole diameter after the failure and D_0 is the original hole diameter. The diameters were measured in two perpendicular directions. Expanded specimen edges were also investigated with a digital microscope.

Unexpanded Hole Edge Investigation. To investigate differences between the initial hole edge conditions, visual inspection was carried out on all hole edge quality specimens. Hole surfaces of the materials were imaged with laser scanning confocal microscopy. Cross-sectional samples (RD-ND) of material near the hole edge were cut, polished, and etched with 2% Nital. Vickers microhardness profiles inwards from the hole edge of the cross-sectional samples were measured with 3 measurements at a given distance from the hole surface. The measurement location in all samples was at quarter thickness from the top surface, and the utilized measurement force was 0.981N.

Results and discussion

Base Material Microstructural Investigation. Determined fractions of RA and material bulk hardness measurement results are presented in Table 1. Significantly higher RA fraction was achieved with the higher IA temperature. Detected local RA fractions were considerably lower in the EBSD measurements compared to the XRD measurements. IAT 650°C material showed higher bulk material hardness accordingly to the lower RA fraction.

Table 1. Fractions of retained austenite and material bulk hardness measurement results. Standard deviations of hardness measurements are given.

Material	Retained austenite content [vol.%]		Hardness [HV10]
	XRD	EBSD	
IAT 650°C	7.5	2.1	331 ± 2
IAT 700°C	43.3	32.4	305 ± 1

FESEM images of material microstructures at quarter thickness are presented in Fig. 1a–b. IAT 650°C material consisted mostly of fully tempered martensite/ferrite with RA and cementite between the laths in addition to carbide precipitation. In IAT 700°C material, the microstructure was a mixture of fully tempered martensite/ferrite and RA with some cementite precipitation.

EBSD phase maps of material microstructures at quarter thickness are presented in Fig. 1c–d. In IAT 650°C material, most of the map consist of martensite/ferrite with some visible small pools of RA. In IAT 700°C material, the fraction of RA in the map is high. Some unindexed spots were left in the maps, which most likely correspond to carbon-enriched constituents such as cementite.

In IAT 650 C material, with high probability, most of the RA is finely divided as interlath austenite between tempered martensite laths, whereas small fraction of RA existed as micro-size pools as shown in Fig. 1c. From Table 1, it can clearly be perceived that the RA fractions differ between the XRD and EBSD methods. These differences in RA fractions are partly due to the resolution limit of EBSD measurements. Finely divided interlath films are undetectable in EBSD and are detectable in XRD. Measurement location can also affect the results of the local determinations, as there is a significant difference between the RA fractions of IAT 700°C material.

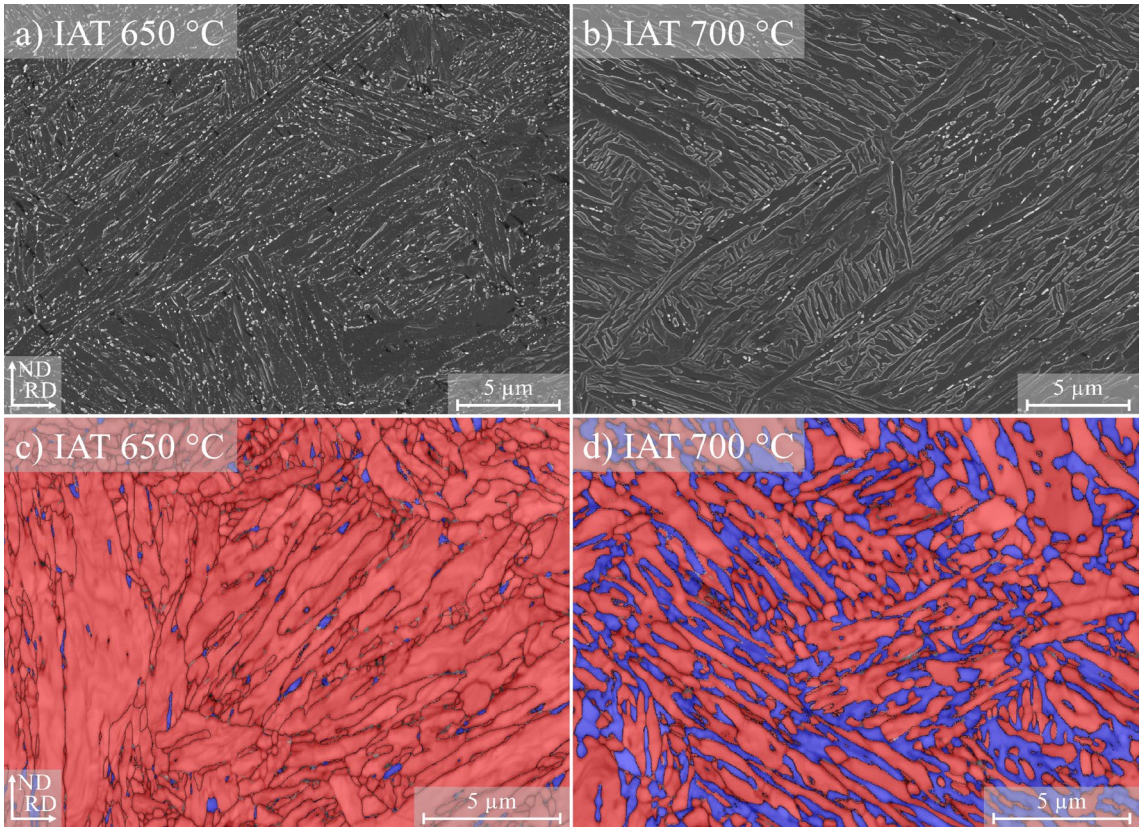

Fig. 1. a–b) FESEM images of quarter-thickness microstructures after 2% Nital etching. c–d) EBSD band contrast, phase, and grain and phase boundary maps of quarter thickness microstructures. Red color corresponds to martensite/ferrite, blue to austenite, black to ≥15° grain and phase boundaries, and grey to unindexed areas.

Tensile Testing. Mean results of tensile testing are presented in Table 2. Lower IA temperature resulted in higher yield and tensile strengths, and simultaneously in lower uniform and total elongations. In IAT 650°C material $n_{4\text{-}6}$ values were also higher indicating greater strain hardening capability, however, yield-to-tensile strength ratios were similar between the materials.

Table 2. Mean tensile and true thickness strain measurement results tested in the longitudinal direction. Standard deviations of the measurements are given.

Material	$R_{p0.2}$ [MPa]	R_m [MPa]	$R_{p0.2}/R_m$ [-]	$n_{4\text{–}6}$ [-]	A_g [%]	A_{50} [%]	$R_m \times A_{50}$ [GPa%]	$\varepsilon_{p\_a_{min}}$ [-]
IAT 650°C	841±8	1027±13	0.82±0.00	0.18±0.00	10.4±0.6	15.8±2.2	16.3±2.4	0.40±0.04
IAT 700°C	774±17	911±10	0.85±0.01	0.11±0.00	16.7±0.4	27.1±0.8	24.7±0.9	0.68±0.03

Thickness strain measurement results are presented in Table 2. IAT 700°C material had higher $\varepsilon_{p\_a_{min}}$ values implying higher tolerance to local deformation, which is also reflected in the higher post-uniform elongation. The fracture surfaces of IAT 700°C specimens were visibly smoother and had more pronounced localization of thinning at the midpoint of the fracture surface compared to IAT 650°C material. Slight local delaminations were observable in the fracture surfaces of IAT 650°C specimens.

Engineering stress-strain curves of the IAT materials tested in the longitudinal direction are presented in Fig. 2a. A yield point plateau is observed in IAT 650 °C material prior to increased strain hardening. In IAT 700°C material, yielding behavior is more constant.

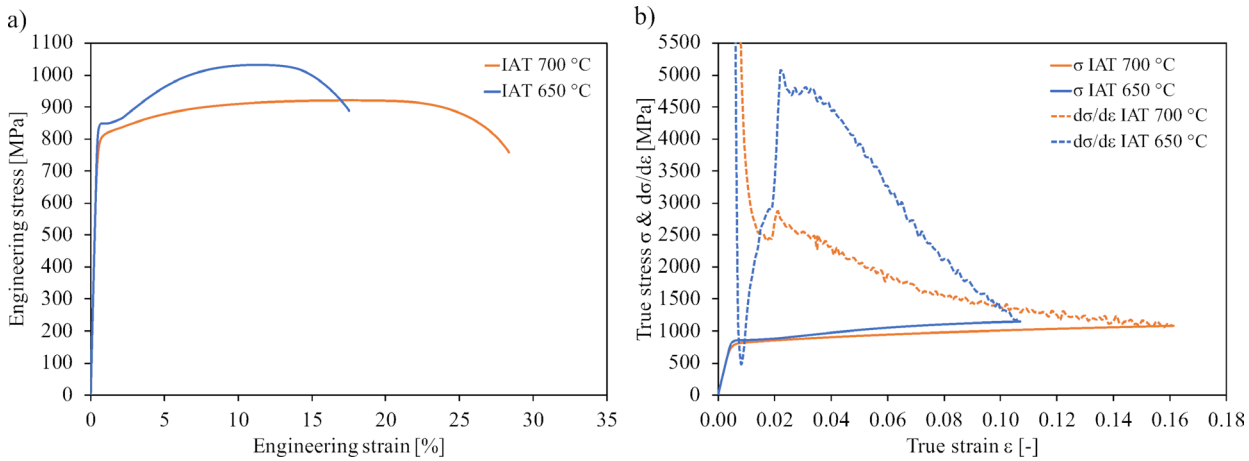

Fig. 2. a) Engineering stress-strain curves and b) true stress-strain curves and strain hardening rates of the IAT materials tested in the longitudinal direction.

True stress-strain curves and strain hardening rates of the IAT materials are presented in Fig. 2b. IAT 650°C material had a significant drop in the strain hardening rate prior to sharp increase to higher values, displaying a pronounced TRIP-effect (transformation-induced plasticity) after the yielding indicating to less stable retained austenite owe to lower IA temperature. In IAT 700°C material, the decrease in the strain hardening rate was steadier. The differences indicate that the stability of the RA is higher in IAT 700 °C material and strain-induced martensite transformation did not occur during the straining the sample. Deformation of ductile austenite enables the high uniform and total elongations in the IAT 700 °C material.

Hole Expansion Testing. Results of hole expansion testing are summarized in Table 3. With the punched hole edge condition, IAT 650°C material had extremely low HER values. In IAT 700°C, the mean HER was slightly higher. With the present testing, it is difficult to decisively state whether this difference is due to increased tensile formability introduced by the higher RA fraction or by the decreased tensile strength, as higher tensile strengths tend to lead to lower mean HER values.

W-EDM edge condition improved HER of both materials, especially IAT 700°C. However, the increase in HER was not as substantial as expected. In hot-rolled complex-phase steels with over 1000 MPa tensile strength, W-EDM HER values over 100% are possible to obtain [5]. High inhomogeneity of the microstructure could have limited the W-EDM HER even when the effects of shear-affected zone are removed.

Table 3. Mean hole expansion test results. Standard deviations of tests with punched hole edge condition are given.

Material	Punched HER [%]	W-EDM HER [%]
IAT 650 °C	4±3	18*
IAT 700 °C	17±4	62

*Failure occurred in an irregular zone in the edge.

In IAT 650°C W-EDM specimen, the failure occurred from a point of unevenness in the edge resulting from the starting/ending point of the hole circumference cutting. Without it, the W-EDM HER value could have been higher, and this should be considered when comparing the HER results. In IAT 700°C specimen, a smaller propagating crack was observed in the similar location, however, the through-thickness crack was located near the material rolling direction. This could indicate that IAT 700°C material is less sensitive to edge defects. As the number of tested

specimens was low due to limited amount of laboratory-rolled material, confirmation would require additional investigation.

In Fig. 3a–d, top-down images of the expanded hole expansion specimens are presented. In the punched specimens, especially for IAT 650°C material, the through-thickness failures occurred prior to proper flange formation. In the IAT 700°C W-EDM specimen with higher HER, flanging was more pronounced. The poor surface quality of the laboratory hot-rolled material is also observable in Fig. 3a–d, with visible spots of furnace scale rolled into the material as scale breaking was not possible between annealing and hot rolling. The surface quality could have had an influence on the hole expansion performance, as the defects can function as strain localizers near the hole edge.

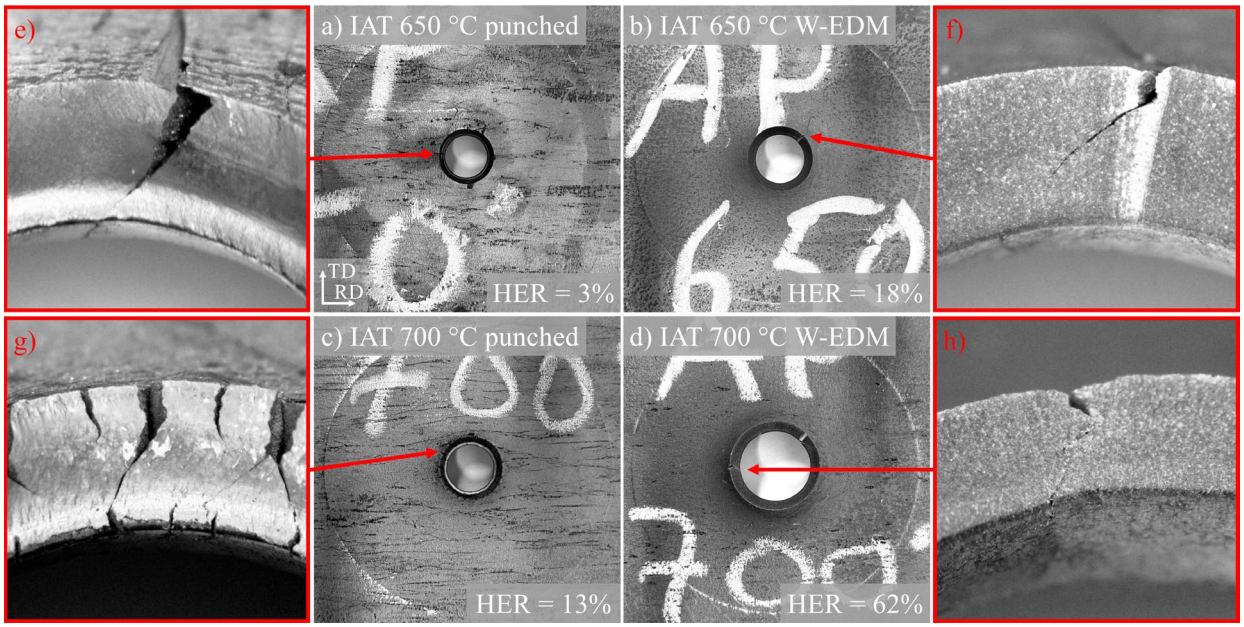

Fig. 3. a–d) Top-down images of hole expansion specimens after the testing. e–h) Close-up images of the through-thickness failures in the hole edges.

In Fig. 3e–f, close-up images of the through-thickness failure locations in the hole edges are presented. Comparing the hole surfaces of the punched specimens, IAT 650°C specimens had smaller number of propagating cracks from the top surface of the test compared to IAT 700°C specimens. In Fig. 3g, small cracks can also be seen propagating from the expanding tool side of the hole edge of the IAT 700°C specimen, and delamination of a surface layer in the IAT 650°C specimen is visible in Fig. 3e. The hole edges of W-EDM specimens were smoother with only a few propagating cracks. Fig. 3f shows the through-thickness crack originating from the irregular zone in the edge of the IAT 650°C specimen. In Fig. 3h, some amount of necking is observable prior to the through-thickness failure of the IAT 700°C specimen. In all specimens of Fig. 3e–f, based on the angle of the through-thickness crack, the final failure is occurring through shearing after the crack initiation.

Unexpanded Hole Edge Investigation. Fig. 4 shows the differences between the hole edge conditions with the different preparation methods prior to the hole expansion testing. Laser microscope surface scans of punched edges are presented in Fig. 4a–b. Burnish-to-fracture zone ratios were low in both materials, 15% for IAT 650°C material and 11% for IAT 700°C material. Fig. 4a–b also shows the fracture surface of IAT 700°C material being comparably rougher. Essentially no burring was observed in the specimens. Slight oxidation was visible in the surfaces of the W-EDM specimens.

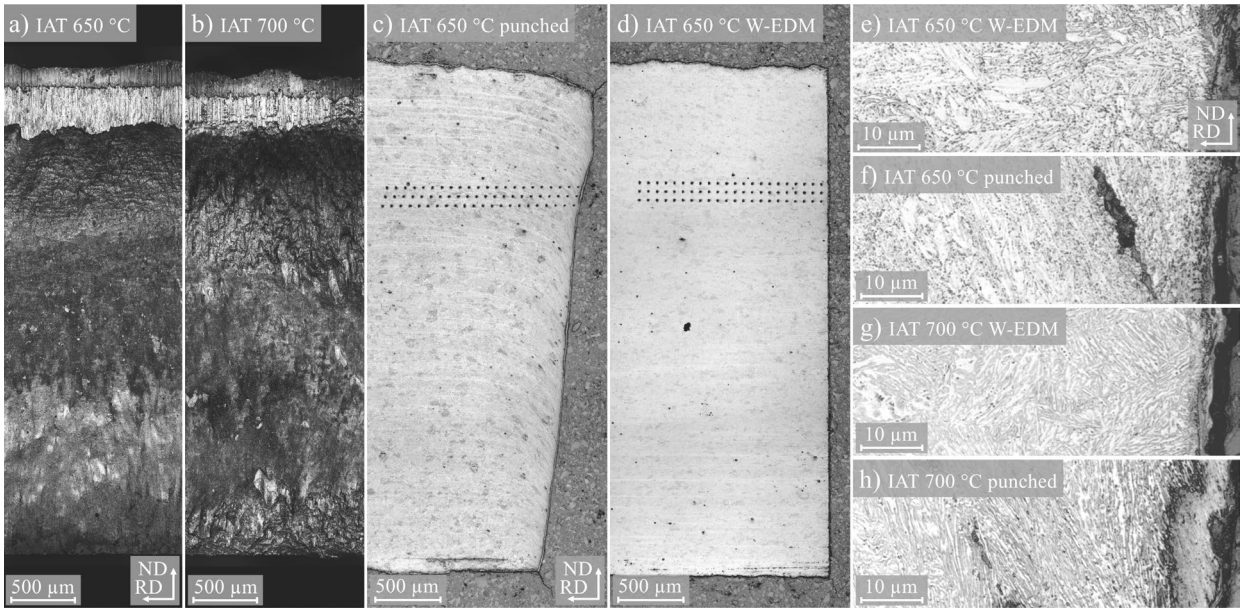

Fig. 4. Images from investigations of unexpanded hole edges: a–b) Laser microscope scans of punched hole surfaces. c–d) Cross-sections of material close to the hole edges. e–f) Laser microscope images of microstructures close to hole edges, 2% Nital etching.

The microhardness measurement lines are visible in the example hole edge cross-section presented in Fig. 4c–d. Nital etching in Fig. 4c also shows deformation of the material towards the sheared edge. Fig. 4d shows the W-EDM edge being considerably smoother compared to rolling surfaces. In Fig. 4c–d, initial delamination of a bottom surface layer is observable. Fig. 4e and g show essentially undeformed microstructure close to the W-EDM edges. Fig. 4f and h show intensive deformation of the microstructure close to the punched edges. Additionally, void formation along the material flow lines can be observed.

Results of microhardness testing of unexpanded hole edges are presented in Fig. 5. No change in the material hardness was observed in the W-EDM edge for both investigated materials. In the punched hole edges, there was a significant difference in the strain hardening of the material near the hole edges between the materials. In IAT 700°C material, the maximum hardness near the edge was higher, and depth of the shear-affected zone was deeper compared to IAT 650°C material. IAT 700°C base material had a major fraction of retained austenite (43.3%) compared to IAT 650°C base material (7.5%). Strain-induced martensite transformation because of high strain rate of the punching process could be a contributing factor to the major increase in the hardness of the punched IAT 700°C sample. The stability of retained austenite is known to be influenced by strain rate dynamics. Therefore, while RA remains stable under tensile loading for the IAT 700°C material, it exhibits instability under applied punching condition. Consequently, while TRIP was not observed during tensile testing, a significant increase in hardness is noted in the punched sample.

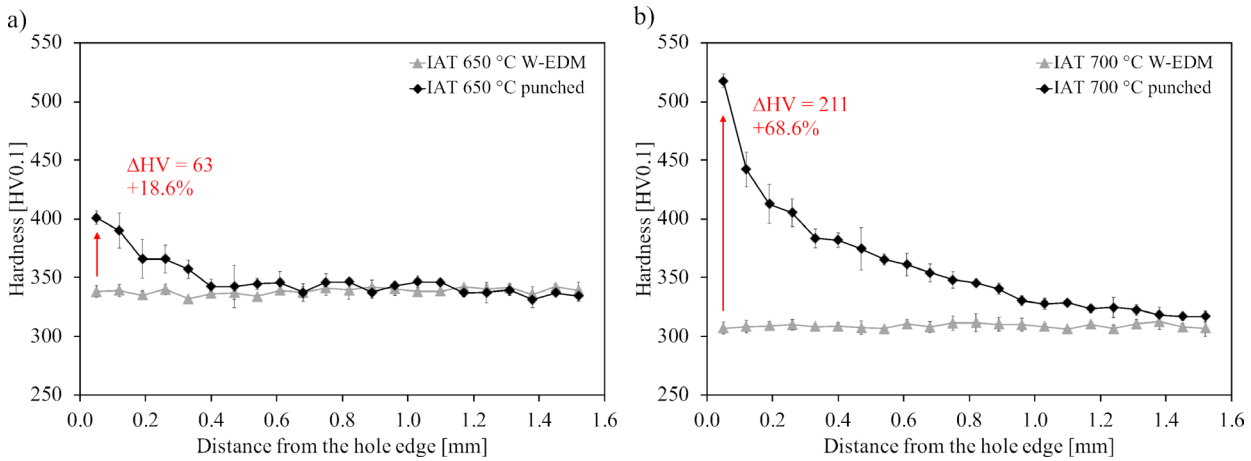

Fig. 5. Microhardness measurement results of the unexpanded hole edges of a) IAT 650°C and b) IAT 700°C materials.

The closest microhardness measurement points were located 50 µm from the hole surfaces. The deformation is more severe closer to the edge as can be seen from the Fig. 4f and h microstructures, thus the actual hardness maximums near the edges can be even higher. For future investigation, it could be beneficial to further examine the fracture surfaces in detail to confirm whether the failure in punching occurs in a more brittle manner in the IAT 650°C material. Additionally, comparisons to edge hardness after the hole expansion testing could provide more insight on the failure behavior of the IAT medium Mn steels with significant RA fraction.

Summary

In this paper hole expansion of a 0.3C–1Si–6Mn–2Al medium manganese advanced high-strength steel was investigated. The steel was laboratory hot-rolled and intercritically annealed (IA) with two IA temperatures to produce different fractions of tempered martensite/ferrite and retained austenite (RA). Tensile tests were performed, and hole expansion tests according to ISO 16630 were conducted to obtain hole expansion ratios (HER) with punched and wire electrical discharge machined (W-EDM) edge conditions.

The results led to following conclusions:

- With the higher IA temperature, material with increased RA fraction and improved tensile strength – total elongation balance was achieved.
- High RA fraction did not lead to drastic improvement of HER in punched materials.
- Punched HER values were poor due to inhomogeneity of microstructure and high amount of strain hardening in the edge.
- W-EDM edge condition improved HER due to removal of shear-affected zone for both materials, the effect was more significant in the material with the higher RA fraction.
- Investigated materials are sensitive to strain rate, which is high in the hole punching process. Stability of RA in shearing should be investigated in further detail.
- Limitations of the laboratory hot rolling compared to industrial production, such as poor surface quality, scale, and temperature variations, could have reduced the hole expansion performance.
- Further optimization of processing and microstructures are required to improve the hole expansion performance of IA treated medium Mn steels.

Acknowledgements

The authors are grateful for financial assistance of the Business Finland research project FOSSA – Fossil-Free Steel Applications. The authors would also like to thank Jane and Aatos Erkon säätiö

(JAES) and Tiina ja Antti Herlinin säätiö (TAHS) for their financial support on Advanced Steels for Green Planet Project.

References

[1] B.S. Levy, C.J. Van Tyne, Review of the shearing process for sheet steels and its effect on sheared-edge stretching, J. Mater. Eng. Perform. 21 (2012) 1205–1213. https://doi.org/10.1007/s11665-011-9997-x

[2] International Organization for Standardization, ISO 16630:2017 Metallic materials – Sheet and strip – Hole expanding test, (2017)

[3] P. Larour, J. Hinterdorfer, L. Wagner, J. Freudenthaler, A. Grünsteidl, M. Kerschbaum, Stretch flangeability of AHSS automotive grades versus cutting tool clearance, wear, angle and radial strain gradients, IOP Conf. Ser. Mater. Sci. Eng. 1238 (2022) 012041. https://doi.org/10.1088/1757-899x/1238/1/012041

[4] A. Karelova, C. Krempaszky, E. Werner, P. Tsipouridis, T. Hebesberger, A. Pichler, Hole expansion of dual-phase and complex-phase AHS steels - Effect of edge conditions, Steel Res. Int. 80 (2009) 71–77. https://doi.org/10.2374/SRI08SP110

[5] W. Cho, B.S. Jeong, K. Jeong, S.H. Lee, H. Kim, J. Lee, S. Kim, H.N. Han, New approach to hole-expansion ratio in complex phase and martensitic steels: Understanding the role of punching damage, J. Mat. Res. Tech. 26 (2023) 837–849. https://doi.org/10.1016/j.jmrt.2023.07.253

[6] J.H. Kim, E.J. Seo, M.-H. Kwon, S. Kang, B.C. De Cooman, Effect of quenching temperature on stretch flangeability of a medium Mn steel processed by quenching and partitioning, Mat. Sci. Eng. A 729 (2018) 276-284. https://doi.org/10.1016/j.msea.2018.05.083

[7] Y.-R. Im, E.-Y. Kim, T. Song, J.S. Lee, D.-W. Suh, Tensile Properties and Stretch-Flangeability of TRIP Steels Produced by Quenching and Partitioning (Q&P) Process with Different Fractions of Constituent Phases, ISIJ Int. 61 (2021) 572-581. https://doi.org/10.2355/isijinternational.ISIJINT-2020-388

[8] N. Fonstein, Advanced High Strength Sheet Steels, first ed., Springer International Publishing, Cham, 2015, XXII 396. https://doi.org/10.1007/978-3-319-19165-2

[9] S. Lee, S.-J. Lee, B.C. De Cooman, Austenite stability of ultrafine-grained transformation induced plasticity steel with Mn partitioning, Scr. Mater. 65 (2011) 225-228. https://doi.org/10.1016/j.scriptamat.2011.04.010

[10] P. Kantanen, S. Anttila, P. Karjalainen, R. Latypova, M. Somani, A. Kaijalainen, J. Kömi, Microstructures and mechanical properties of three medium-Mn steels processed via quenching and partitioning as well as austenite reversion heat treatments, Mater. Sci. Eng. A 847 (2022) 143341. https://doi.org/10.1016/j.msea.2022.143341

[11] International Organization for Standardization, EN ISO 6892-1:2019 Metallic materials. Tensile testing. Part 1: Method of test at room temperature, (2019)

[12] VDA 238-110. Verband der Automobilindustrie e. V., VDA 238-110 Ermittlung der Lokalen Duktilität aus der Bruchfläche von Zugproben / Determination of Local Ductility by Fracture Surface Analyses of Tensile Test Specimens 08/2023, (2023)